UNCLASSIFIED

AD 402 121
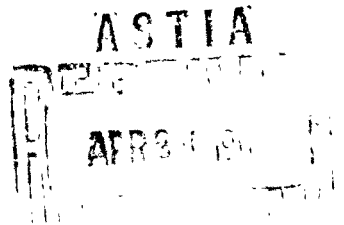
UNCLASSIFIED

63-3-2

ASD-TDR-63-14

● **Power Sources For Directed Energy Weapons**

Sixth Quarterly Report

ASD Technical Documentary Report No. ASD-TDR-63-14

APRIL 1963 ● AFSC Project 3805

ASTIA

AFR3

DIRECTORATE OF ARMAMENT DEVELOPMENT

Det 4, AERONAUTICAL SYSTEMS DIVISION

AIR FORCE SYSTEMS COMMAND ● UNITED STATES AIR FORCE

EGLIN AIR FORCE BASE, FLORIDA

ACKNOWLEDGEMENT

ABSTRACT

A discussion is given of initial test results obtained on a superconducting toroidal coil and a thermal discharge switch.

Critical currents of the toroid are very high at low fields but considerable current degradation was observed at fields in the order of 15 kilogauss.

Initial test results on the thermal switch indicate that the time required for a thermal transition is rather long ($\frac{1}{2}$ sec). More tests are to be performed, including an investigation of magnetic transitions.

Some discharge experiments have been performed. Low energy discharge pulses with a rise time in the order of 2 msec have been obtained.

Experiments are described in which the vacuum breakdown voltage as a function of electrode separation were measured for 304 stainless steel electrodes having essentially planar geometry, for similar electrodes having the cathode coated with a variety of materials, and for electrodes having sphere-to-plane geometry. Electrode separation was varied between 20 and 1 cm, while the ambient gas pressure was either about 10^{-4} or 10^{-7} torr.

In other experiments at these pressures, the voltage support capability of the high voltage bushing has been measured when it is terminated by field intensification discs (having an edge of known radius of curvature), and when some of the bushing's glass insulator rings are protected by two truncated cones. A urethane grading resistor having a specific resistivity $\sim 1 \times 10^{11}$ ohm-cm was used in one of the bushings during some of these tests.

The 400 kv HIVE facility, in which complementary vacuum breakdown studies will be carried out, has been assembled and the high voltage bushings satisfactorily tested. Latest progress in the development of the Type II high voltage bushing is described. It is hoped to voltage-test the first of these bushings shortly.

CONTENTS

ILLUSTRATIONS

TABLES

1. LOW TEMPERATURE ENERGY STORAGE

1.1   INTRODUCTION

Procurement of dewars, transfer tube, liquid helium container and auxiliary equipment was completed and some experiments with superconductors have been performed. Difficulties were encountered in winding a toroidal coil with 0.010" Nb-25% Zr wire. Winding of a coil designed for 22,000 turns was discontinued after 13,860 turns because of difficulties handling this wire on a toroid winding machine. The winding was further complicated by the number of taps required and the mylar insulation between layers. However, some useful information could be obtained on this coil at fields up to 15.8 kilogauss and a new and improved coil design for higher fields was completed.

Difficulties were also encountered with contacts between superconducting wires and between superconducting and normal wires. This has caused initial test results to be influenced by quenching in the contacts. Better techniques of making contacts have been developed and a further investigation of contacts is in progress.

The experimental program was divided in three areas:

- Superconducting Magnet Coils
- Superconducting Switch
- Energy Discharge

A thermal switch was constructed and tested. Although the testing has not yet been completed, the results indicate that this method of switching is probably too slow for the type of discharges desired. A similar switch, but operating on the basis of magnetic transitions, will be made and tested. This method is likely to result in much faster switching.

The discharge experiments have only recently been started and no conclusions can be drawn from the test results obtained thusfar, other than that some low energy discharge pulses with rise times in the order of 2 msec have been obtained.

The objective of this report is to present and discuss the test results obtained and to outline the experimental program intended for the next quarterly period.

2. SUPERCONDUCTING COIL

Energy may be stored in cylindrical or toroidal coils and these coils may have circular or rectangular cross sections. Thus far only coils with circu- lar cross sections have been considered. The toroidal coil looks more attractive since it fully contains the magnetic field and the absence of end effects may result in a reduction of current degradation effects which have been encountered with superconducting solenoids. Therefore a toroidal coil was wound and the I_c versus B curve for this coil was investigated. Several taps were made in the winding to allow measurements of critical currents at various field strengths. The dimen- sions of the coil are shown in Fig. 1 and the winding data is given in Table I.
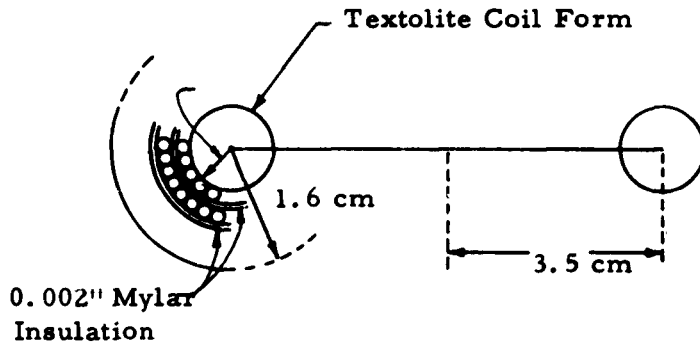
Fig. 1   Superconducting Toroid Wound with 0.010"Nb-25%Zr Wire

TABLE   I

Winding Data and Critical Currents of Superconducting Toroid

Winding	Turns	I_c(amps)	B (gauss)
1-2	660		
1-3	1,269		
1-4	2,971	41.5	8,200
1-5	4,470	28	8,350
1-6	6,460	22	9,500
1-7	8,160	19.5	10,600
1-8	9,860	18	11,850
1-9	11,860	17	13,500
1-10	13,860	17	15,800

For this toroid the maximum magnetic field strength occurs at a distance of 3×10^{-2} meter from the center A and is given by:

$$B = \mu_o n I \qquad Webers/m^2 \qquad (1)$$

where: $\mu_o = 4\pi \times 10^{-7}$ Henries/m

$$n = \frac{N}{2\pi l} = \frac{total \ number \ of \ turns}{2\pi (3 \times 10^{-2})}$$

Thus:

$$B = \frac{4\pi \times 10^{-7}}{2\pi \times 3 \times 10^{-2}} NI = \frac{2}{3} \times 10^{-5} NI \qquad (2)$$

or in gauss:

$$B = 0.0667 \ NI \ gauss \qquad (3)$$

B versus I plots for each of the taps according to (3) are shown in Fig. 2. A plot of the critical points on each of these curves represents the I_c versus B transition curve. The critical currents were measured using the circuit shown in Fig. 3.

The resistor R_1 is composed of graphite plates, mounted in parallel, about 1 cm apart, and submerged in a NaCl solution. The resistance can be varied uniformly by varying the level of the NaCl solution.

The measurements were taken by connecting terminal a to the desired tap and cooling the coil to 4.2°K. The current is then slowly increased by means of R_1. When the critical current I_c is reached, the coil goes normal and its high resistance causes the battery current to flow through R_2. A low value of R_2 is chosen to prevent high induced voltages from building up in the coil. Low resistance shunts may also be connected between the other taps. The measurements were repeated for each of the taps.

The equipment used is shown in Fig. 4. The toroidal coil, mounted between two textolite disks is shown in Fig. 5 (the coil mounted on the left is a thermal switch which will be discussed later).

As previously indicated, the coil was intended to be wound for a field of about 25 kilogauss. Difficulties in handling NbZr wire on a toroid winding machine, together with difficulties handling a large number of taps and mylar insulation between each layer of wire, prevented this field from being attained. This is because a field of 25 kilogauss would have required a coil with about 22,000 turns instead of the 13,860 obtained. A new coil has been designed with less taps and using heavily insulated wire which does not require mylar to be wound between layers. With this coil it is expected that the I_c versus B curve of Fig. 2 can be extended to about 30 kilogauss.
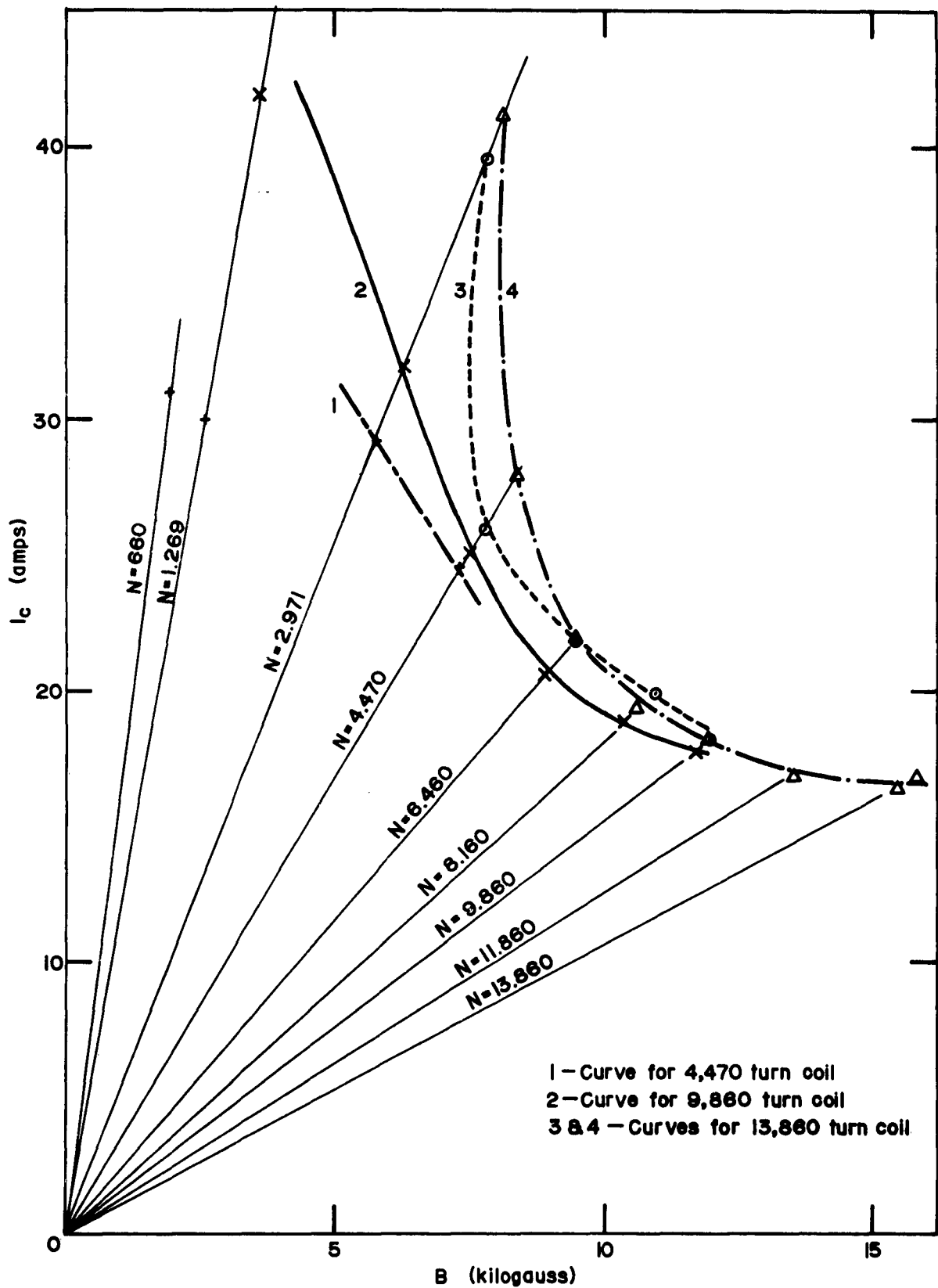
Fig. 2 Critical Current vs. Magnetic Field Curves for Toroidal
Coils Wound with 0.010" Nb—25%Zr Wire, Operating at 4.2°K

4

At Liquid Helium Temperature

S = Low Current Switch
R_1 = High Current Variable Resistor
R_2 = Shunt Resistor of 0.25-1Ω
A_1 = D.C. Ammeter, 0-50 amps
A_2 = D.C. Ammeter, 0-50 amps

12 V Battery

Fig. 3   Test Circuit for Critical Current Measurements

Fig. 4   Cryogenic Test Facility

6
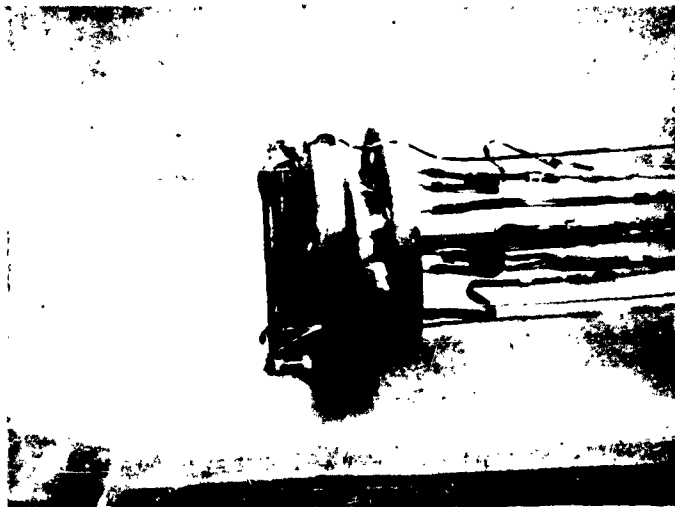
Fig. 5   Toroidal Coil and Thermal Switch Assembly

Curve 1 in Fig. 2 was obtained when the toroid was wound with a total of only 6, 460 turns. The turns were then increased to a total of 9, 860 turns and the test results are plotted in curve 2. Finally curves 3 and 4 were obtained after all 13, 860 turns were wound. Curves 1, 2, 3 and 4 would be expected to coincide. This is approximately true for fields higher than 10 kilogauss. However, at lower fields large deviations occur. This is most likely to be caused by training. The same effect on toroids was observed by Montgomery[1] who found that at low fields, repeated current transitions at a given magnetic field cause the coil to be trained to carry higher currents. Training has also been observed by LeBlanc and Little[2] in cold worked niobium samples and by Hulm[3] and other authors in solenoids.

There appears to be a difference between the phenomenon of training observed in both cases. While in solenoids and short wire tests the training is greatly influenced by the metallurgical history of the specimen and can occur at any value of magnetic field, a comparison with the results obtained on toroids suggests that this effect is more stable in toroids and occurs only at low fields below about 10 kilogauss. Training, though widely observed and reported, is not very well understood at this time. From a practical point of view it does not seem to be a serious problem as this effect can be easily stabilized by conducting a number of superconducting to normal transitions and it stabilizes at high critical currents.

The points obtained for curve 1 at N= 660 and N= 1269 deviate widely from the expected curve. Although this could also be attributed to training, it was more likely caused by premature quenching in one or more of the wire contacts. As previously indicated, difficulties were encountered in making contacts. Even a very small contact resistance coupled with the relatively high currents, causes localized heating which in turn causes the contact to go normal. Once a normal region occurs, it is rapidly propagated throughout the entire coil making it difficult to distinguish between this type of quenching and quenching initiated by the field at the inside layers of wire. Contacts between NbZr wires should be preferably superconducting, i.e., no contact resistance at all. This is possible by means of spot welding. However, the 'hard superconductor' properties of NbZr wire are a result of extensive cold working causing internal mechanical stresses. Welding causes these stresses to be relieved. As a result a welded contact can carry high currents but only at low external fields. Such a contact must therefore be made outside the coil. Ano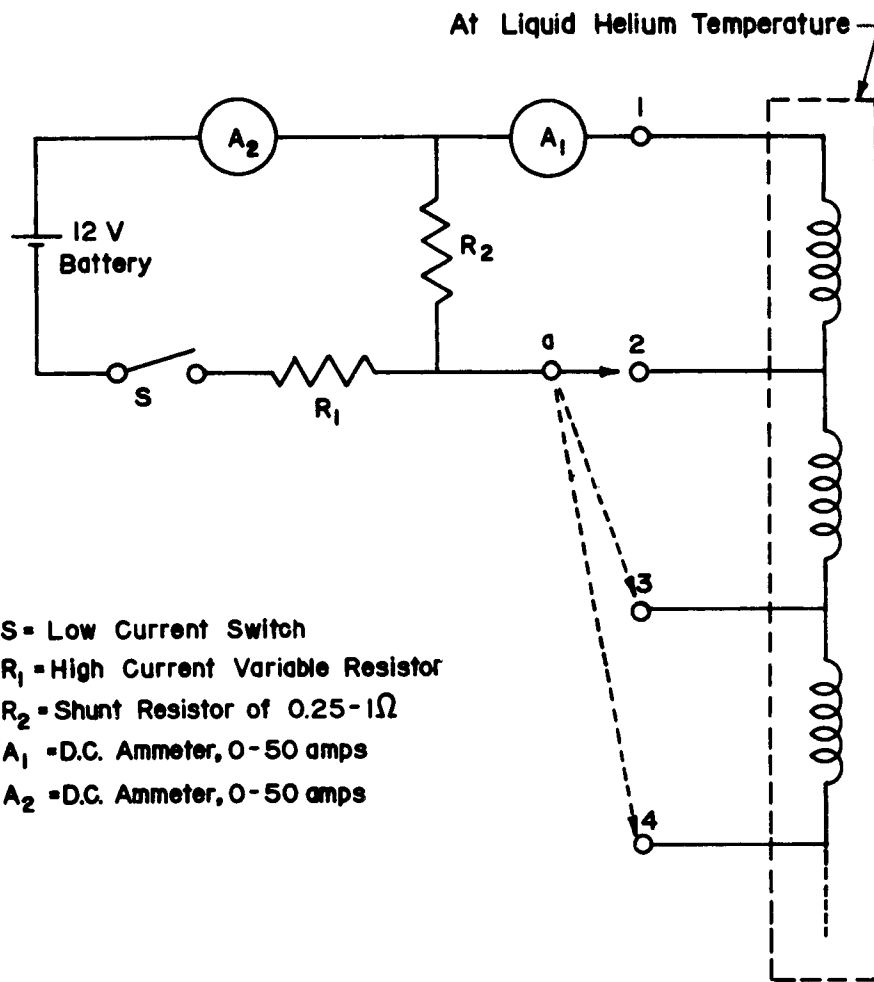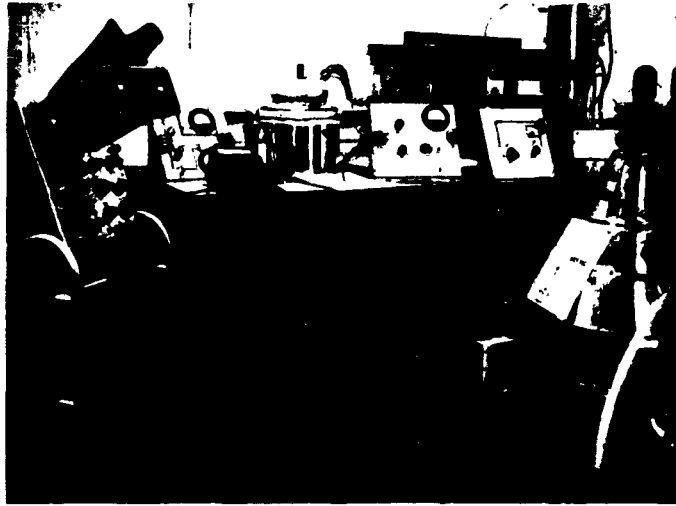ther possibility is pressure contacts using large contact areas. It is rather difficult to obtain the same critical currents as obtainable in the wire for such contacts. A third method involves cold welding, if this is possible. This is presently being investigated. The NbZr to copper lead connections were made by means of pressure contacts having very low contact resistance. The contact and a certain length of NbZr wire were then fully exposed to the liquid helium, thus acting as a heat sink and preventing heat from being conducted into the coil. A further investigation of contacts is being made and will be reported in a subsequent report.

It would be interesting to compare the I_c versus B curves as obtained on toroids and solenoids. However, such a comparison, in order to be of some value, must be based on coils of very similar construction with respect to space factor, inside winding diameter, volume, etc. No solenoid was available for such a comparison. In order to get some indications, a comparison is made with a typical solenoid curve as published by Hulm[3] and is shown in Fig. 6. These curves indicate that at high fields, greater than 12 kilogauss, there is not much difference, while for low fields the critical currents in the toroid are considerably higher. The fact that no higher critical currents were obtained at high fields seems rather disappointing although this effect should be reconfirmed to make certain that the measurements are not influenced by quenching in the wire contacts. Furthermore, it is possible that under more similar conditions the toroid would compare favorably with solenoids.

Montgomery[1] indicated that the 'degradation' of the I_c versus B curve is greatly dependent upon the space factor

$$\lambda = \frac{\text{volume of wire}}{\text{total coil volume}}$$

For coils of similar type and somewhat similar dimensions, the following relation seems to hold with some degree of accuracy:[2]

$$\lambda I_c = C \text{ (constant)} \tag{4}$$

A comparable solenoid[2] with an inner diameter of 1.26 cm and wound with 0.010" Nb-25%Zr wire, had a critical current of I_c= 19 amps at B= 18 kilogauss. This solenoid has a space factor of λ = 0.48. The average space factor of the toroid is estimated to be 0.28. However, due to the method of winding, this space factor is not uniformly distributed and is about 0.55 at the inner circumference where the highest field exists and where quenching is initiated. Assuming that (4) holds for toroids, the critical current of a toroid having a λ = 0.48 at the inner circumference would be

$$I_c = \frac{0.55}{0.48} \times 16.5 = 19 \text{ amps at 18 kilogauss.}$$

Assuming a critical current of 16.5 amps for the present toroid at 18 kilogauss, this is exactly the same as reported by Montgomery for a solenoid.

The stored energy is:

$$E = \tfrac{1}{2}L I_c^2 \tag{5}$$

L is the coil inductance in henries, and is proportional to N^2, while N is proportional to λ. Thus

$$E \propto \lambda^2 \left(\frac{C}{\lambda}\right)^2 \tag{6}$$

9
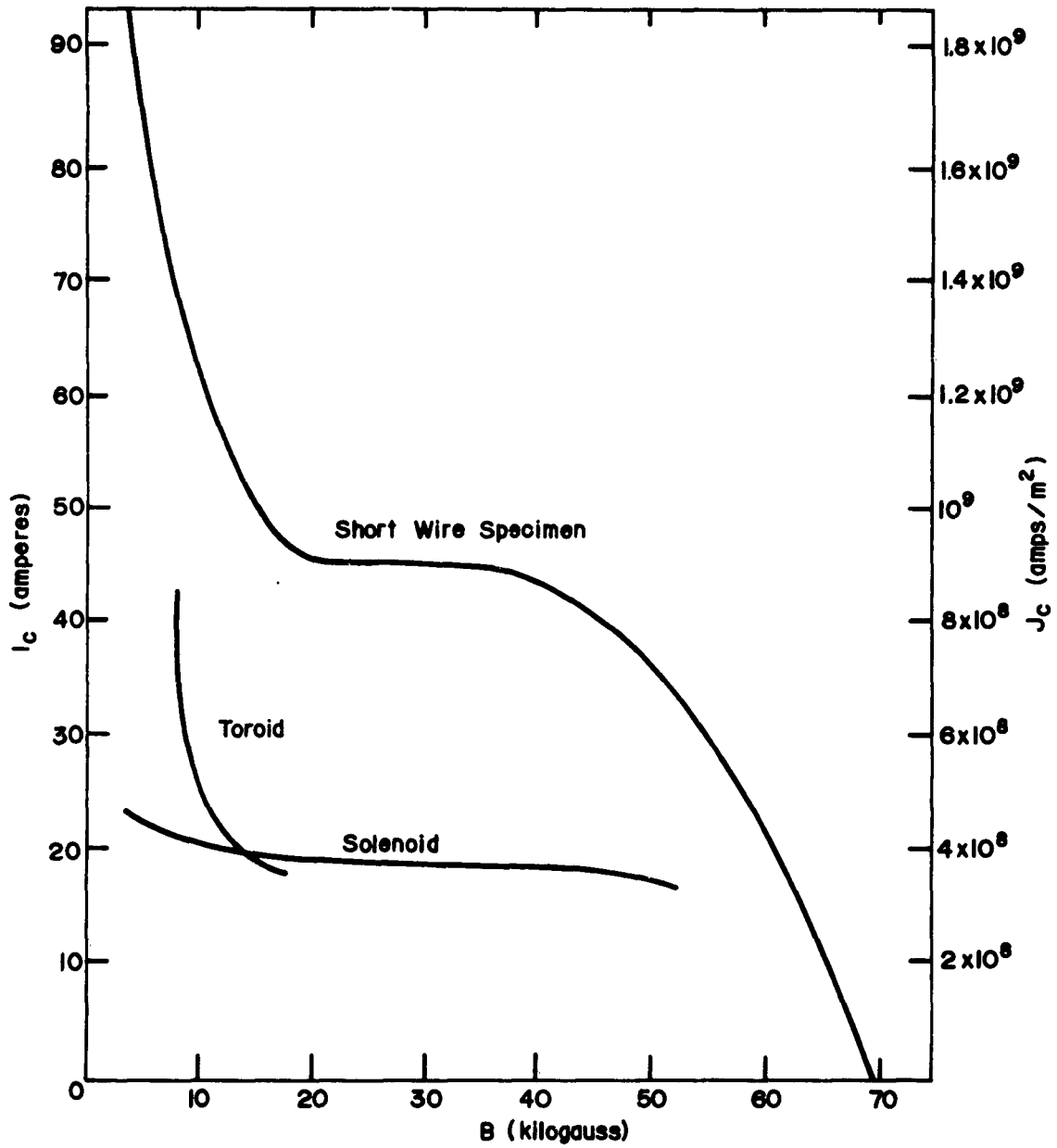
Fig. 6 Critical Current of Short Wire Sample,[4] Solenoid[4] and Toroid versus Self Generated Magnetic Field for 0.010" Nb−25%Zr Wire

This indicates that assuming Eq. (4) is fairly accurate and also holds for a toroid, the stored energy is independent of λ. However, Eq. (4) only applies for critical currents up to the critical current of a short wire, which is about 45 amps at 18 kilogauss. For the toroid we found:

$$C = 0.55 \times 16.5 = 9.1 \text{ amps} \tag{7}$$

To obtain short wire performance

$$\lambda = \frac{C}{I_c} = \frac{9.1}{45} = 0.202 \tag{8}$$

In other words, according to Eq. (8) short wire performance may be obtained in a coil having a uniform space factor of $\lambda = 0.202$. As a first approximation the energy storage in such a coil would be the same as obtainable in a more densely wound coil, but other factors influencing energy storage densities, such as the inductance in the superconducting state are still to be considered. Furthermore, the conclusions reached are very preliminary and require further experimental verification.

2.1 SELF INDUCTANCE

In the above derivations L has been assumed to be proportional to N^2 and a function of the coil geometry only. This is true for coils in the normal state. As pointed out in Ref. 4, L is also a function of B in the superconducting state. This is caused by the Meissner effect[5] and the mixed state in hard superconductors.[3] These effects cause the inductance in the superconducting state to be lower than in the normal state. This inductance drop is probably less than 10% for fields near the critical field but high for very low fields. A plot of L versus B for a small, densely wound coil was published by Hulm.[3] However, this curve may be assumed to be strongly dependent on the coil geometry and winding density λ. Since the stored energy is directly proportional to the inductance L, an investigation of L in the superconducting state for solenoids and toroids is in order. Present efforts are directed towards determining L in the normal state and comparing this value with $L = f(B)$ in the superconducting state.

2.1.1 Self Inductance in the Normal State

Accurate expressions relating L to the coil dimensions and N^2 for solenoids are discussed in various text books and present no problem. Similar expressions for air core multiply wound toroidal coils are not available.

The inductance of a single layer torus is given by:

$$L = \mu_0 N^2 (a - \sqrt{a^2 - a_1^2}) \text{ henries} \tag{9}$$

where:

$a =$ radius of torus in meters
$a_1 =$ core radius in meters
$\mu_0 =$ $4\pi \times 10^{-7}$ henries/meter

11

In the previous quarterly report[4] the inductance of a multiply wound torus was estimated by using for a_1 the average coil diameter. While this may provide a good order of magnitude estimate, it is not sufficiently accurate for purposes of this investigation. A more accurate method involves the calculation of individual layer inductances and mutual inductances.

The mutual inductance between two layers with radii a_i and a_j as shown in Fig. 7 is:

$$L = \mu \cdot N_i N_j \left(a - \sqrt{a^2 - a_{ij}^2} \right) \text{ henries} \tag{10}$$

where

$$a_{ij} = a_i \text{ for } i < j$$

$$a_{ij} = a_j \text{ for } j < i$$
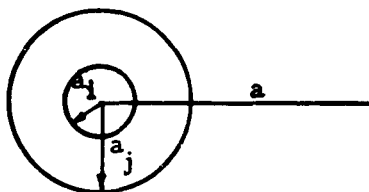
Fig. 7   Toroidal Coil

A coil with a circular cross section and a circular wire build up has been assumed. This is the type of coil that has been wound and is shown in Fig. 1. On the basis of Eq. (10) the total inductance can be represented by

$$L = \sum_{i}^{n} \sum_{j}^{n} L_{ij} \tag{11}$$

where n is the nth layer of a torus of n layers. Since

$$L_{ij} = L_{ji} \text{ for } i \neq j$$

$$L = \sum_{i=1}^{n} L_i + 2\sum_{j=2}^{n} L_{i,j} + 2\sum_{j=3}^{n} L_{2,j} + \dots \dots 2\sum_{j=n-1}^{n} L_{n-2,j} \tag{12}$$

where the first term represents the self inductance of the torus and the remaining terms the mutual inductances.

$$L_i = \mu \cdot N^2 \left(a - \sqrt{a^2 - a_i^2} \right) \tag{13}$$

$$L_{k,j} = \mu \cdot N_k N_j \left(a - \sqrt{a^2 - a_j^2} \right) \tag{14}$$

12

In order to obtain an expression for L in terms of the basic parameters the summations may be approximated by integrals, which yields a series which in turn can be combined and once more approximated by an integral. This calculation is quite laborious and its accuracy subject to experimental verification. Furthermore, the type of coil considered has a non-uniform distribution of the winding density λ, with λ high along the inside circumference of the coil and low at the outside circumference. Tests have indicated that a uniform λ but possibly lower than presently obtained at the inside circumference, is desirable. Such a coil can be wound allowing a closer packing at the outside circumference and allowing the turns on the inside to overlap. Copper clad wire may be selected for this purpose. However, this type of coil would have a non-circular build-up and new equations would have to be set up to calculate the inductance. Such a calculation would be far more complex than the one discussed. An attempt was therefore made to measure the inductance in the normal state. However, no good measurement was obtained. The coil impedance looks as follows:

L = 0.3 H (approximately, from calculations)
R = 10 k Ω measured
C = 10^{-8}F measured at 10 kc

Obviously the Q of this coil is too low to allow a measurement of L at low frequencies while at high frequencies the influence of the coil capacitance is prohibitive. However, the use of copper clad wire is being considered and this should make a low frequency inductance measurement possible (low resistance on account of the copper cladding).

2.1.2   Self Inductance in Superconductive State

The inductances in the superconductive state have been measured using a standard General Radio Bridge operating at 1000 cycles, and are listed in Table II. For reference some calculated inductances in the normal state have been included in Table II. The measured inductances were obtained at low B. Because of L being a function of B, the measurements should be repeated at various levels of B, or by superimposing DC currents of various magnitude upon the current supplied by the bridge.

TABLE II

Toroid Inductances at 4.2°K and 293°K

Winding	N (turns)	L@ 4.2°K (measured)	Approx. L @ 293°K(calculated)
1-2	660	0.3 ±0.1 mh	0.27 mh
1-3	1269	0.6 " " "	
1-4	2971	4.1 " " "	
1-5	4470	9.8 " " "	12.9 "
1-6	6460	21.5 " " "	
1-7	8160	37.0 " " "	
1-8	9860	58.0 " " "	73.0 "
1-9	11860	90.0 " " "	
1-10	13860	136.0 " 10 "	300.0 "

13

Alternately, the inductance could be determined from a time constant measurement as shown in Fig. 8.
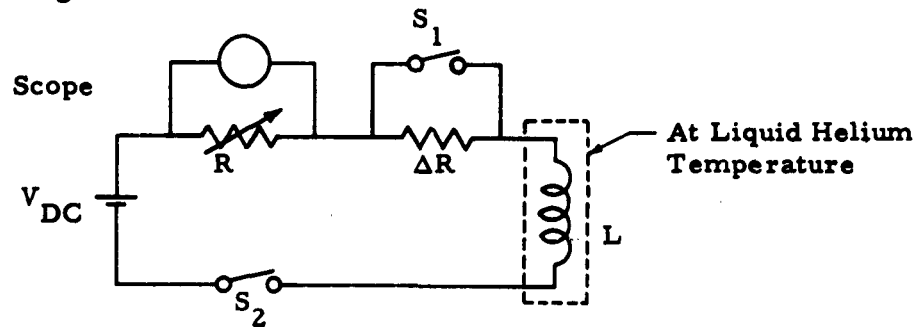
Fig. 8 Test Circuit to Measure Self-Inductance as a Function of the Magnetic Field

Using this circuit, the exciting current of the coil, and thus B, can be adjusted to any desired level. A subsequent change by ΔR of the total series resistance causes the exciting current to change with a time constant determined by the total series resistance (known) and the self inductance of the coil. Since not enough measurements have been made, the results of these tests will be discussed in a future report.

2.2   FUTURE PROGRAM

A new toroidal coil has been designed using a textolite core with a main diameter of 9 cm and a ring diameter of 1 cm. After winding, this would represent the largest coil that can be accommodated in the present dewar system. The number of taps has been reduced to three and the mylar insulation was deleted in favor of using 0.004" wire insulation instead of the standard 0.001". The coil will be wound with a uniform winding density λ and thus will have a non-circular winding cross section. The λ for this coil is estimated at $\lambda = 0.5$. This would yield an estimated $I_c = 20$ amp. This size torus would accommodate an estimated 30,000 turns of 0.014" overall diameter. This results in a maximum field of

$$B = \mu_o \ \frac{NI_c}{2\pi a} = \frac{4\pi \times 10^{-7} \times 30,000 \times 20}{2\pi \times 4 \times 10^{-2}} = 3 \ \text{Webers/m}^2$$

or

$$B = 30,000 \ \text{gauss}$$

At an estimated inductance of 5.3 henries, the total stored energy is

$$\tfrac{1}{2} L I_c^2 = 1060 \ \text{joules}$$

The same field may be obtained using 15,000 turns of copper-clad wire operating at $I_c = 40$ amp . Assuming that this is verified by future experiments, the difference in energy storage would be determined by the $L = f(B)$ characteristics of copper clad--versus plain NbZr wire.

14

Another program which will be pursued is the testing of short wire specimens. Due to variations in the quality of the wire supplied, an accurate comparison of the behavior of solenoids and toroids with short wire samples, cannot be made by using published I_c versus B curves. A 30 kilogauss solenoid has therefore been made and a test arrangement is being set up to perform such tests. Furthermore, the solenoid can also be used for coil analysis and discharge experiments.

3. SUPERCONDUCTING SWITCH

3.1   THERMAL SWITCH

A thermal switch as shown in Figure 5 (cylindrical coil on the left) was designed using 0.005" Nb-25%Zr wire. The wire was wound into a non-inductive coil by reversing the direction of winding for every layer. Copper wire #37 AWG was used as a heat source and was also wound in the form of a non-inductive coil. To provide uniform heating a layer of copper wire was placed between every two layers of NbZr wire. All layers were separated from one another by 0.002" mylar insulation. The windings were wound on a 1/4" diameter x 3 3/4" long textolite core. The coil consists of about 30,000 turns of 0.005" Nb-25%Zr wire and 10,000 turns of copper wire. Despite reversing the direction of winding every layer, an unavoidable buildup at the ends led to a net residual inductance of 0.2 millihenries for the NbZr coil and 0.8 millihenries for the Cu coil. However, these values are sufficiently low to allow operation of the coil at very low fields and thus at a high critical current. This is very desirable because the switch must carry the full coil current in the superconducting state and must have a very high DC resistance in the normal state and should thus be wound with a small wire size.

Critical current measurements indicated I_c= 22 amps. This critical current is adequate for testing purposes, but is lower than would be expected for a non-inductive coil using 0.005" NbZr wire. This is probably caused by current degradation due to proximity effects. Figure 6 indicates that a toroidal coil would provide a much higher I_c at the very low fields encountered in a non-inductive coil. However, it is not so much the critical current which is of interest at this time, but rather the switching time of a thermal transition.

TABLE III

Resistance Measurements on Superconducting Switch

Temperature	300°K	77°K	≃20°K	4.2°K
Nb-25%Zr coil	21 k Ω	17.5 kΩ	10 kΩ	0
#37 AWG Cu Coil	680 Ω	80 Ω	----	6.5 Ω

The measured coil resistances are shown in Table III. The switching time was measured using the circuit shown in Figure 9. Circuit A (detecting circuit) consists of a series arrangement of a 10 k Ω resistor and the superconducting wire of the switch. When S_1 is closed, a voltage of 12 volts appears across the 10 kΩ resistor. When the NbZr wire goes normal, this voltage drops to 6 volts and the rate of change is observable on the scope. The NbZr wire can

be made to go normal thermally by activating circuit B (heater circuit).
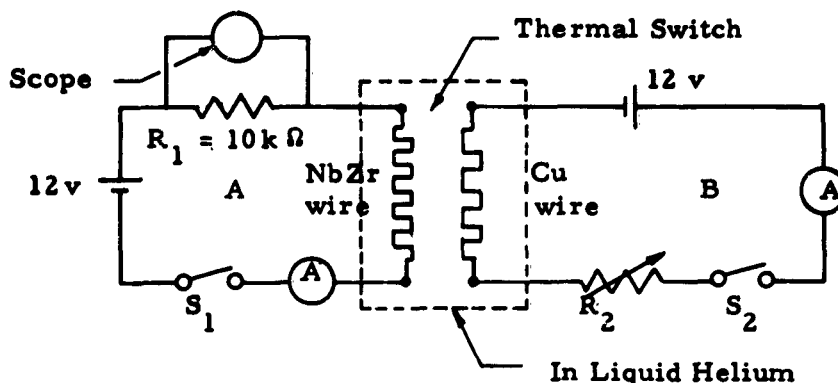
Fig. 9   Test Circuit for Thermal Switch

An oscillograph of such a transition, represented by the voltage drop across R_1 is shown in Fig. 10. The switching time is quite long (about 1/2 second), however, a value of 1.4 k Ω is attained in about 30 milliseconds. Furthermore, it should be noted that the switch was operated at a very low initial current (1.2 ma). If the switch is used in conjunction with a superconducting storage coil, the initial current will be close to the critical current and will generate some heat as it falls off with increasing resistance during a transition. This is likely to result in much faster switching times, and will be further investigated. However, it is not likely that sufficiently fast switching can be obtained in this manner. The reason for this is most likely the thermal inertia together with the filamentary nature of superconductivity in NbZr. Since there is practically no external field, such a switch could just as well be built using soft superconductors such as niobium.   Since superconductivity in these materials is limited to a very thin layer at the surface of the wire, the thermal or magnetic transition would probably be much faster.

$E = 1\frac{1}{2}$ V/scale div.
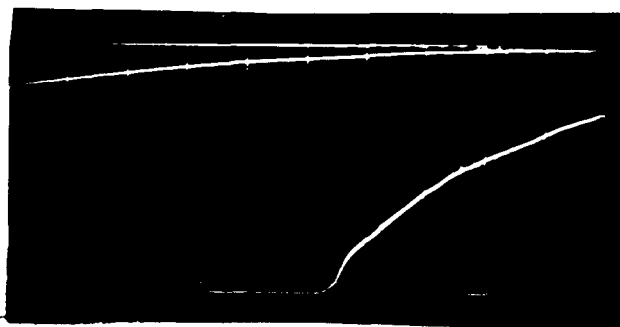
t = 0.05 sec/scale div.

Fig. 10   Voltage Drop in Series Resistance Caused by
Thermal Transition

3.2　MAGNETIC SWITCH

Such a switch would not be much different from a thermal switch except that the transition will be initiated by a magnetic field exceeding the critical field for the current in the main coil.　With reference to Fig. 9, such a switch could be obtained by replacing the Cu winding by another NbZr winding (control winding) and wound inductively.　An experiment along these lines will be prepared in the near future.

3.3　SUPERCONDUCTING CONTACTS

The feasibility of a mechanical superconducting switch will depend largely on the ability of superconducting contacts to carry high critical currents and their subsequent ability to be opened rapidly.　The first part of the experimental program is only concerned with critical current measurements of large area superconductor to superconductors contact as a function of contact material, surface films, contact pressure and contact surface conditions.　One experiment was attempted but failed due to improper line-up of the contacts.　A redesigned contact holding--and spring arrangement to vary contact pressures--is shown in Fig. 11. The contacts consist of 2 x 5 x 1/2 cm niobium bars (2).　Future experiments will be performed using lead and other superconducting contact materials.　Previous work by Meissner[6, 7] has indicated that load bearing areas of the order of 10^{-4} cm^2 yield transition points; i.e., points where the contact resistance changes from 0 to some finite value, in the order of milliamperes.　Consequently, it is anticipated that load bearing areas in the vicinity of 1 cm^2 will yield transition points in the ampere region.　This is likely to depend very much on the contact pressure and the condition of the contact areas.　It is possible that for reasonable contact pressures, the load bearing area obtained will not lead to contact areas which are large enough for transitions to take place in the amp region. It is therefore anticipated that highly polished Nb surfaces will be needed.

3.4　FUTURE PROGRAM

As previously indicated the critical current of the thermal switch was 22 amps which is lower than expected for 0.005" NbZr wire. This may be caused by proximity effects leading to current degradation. It may also be caused by quenching in the contacts.　Initially much lower currents were measured on account of contact resistance and it was found that making contacts with 0.005" wire is much more difficult than with 0.010" wire. Furthermore, the layer insulation has caused a buildup of wire at the ends of the coil which may have resulted in local fields of 1 to 2 kilogauss.　This will be investigated in more detail.　In addition, switching times will be determined at initial currents just below the critical current. This will establish the switching characteristics of such a device when used for energy discharges.　The investigation may then be continued using wires of soft superconducting materials.　However, before such a program is initiated, experiments will be performed on magnetic switches.　The investigation of critical currents in superconducting contacts has been started and will be continued.

ION PHYSICS CORPORATION

CONTACT
RESISTANCE
TESTER

LIST OF MATERIAL

SECTION 'A'-'A'

SECTION 'B'-'B'

SECTION 'C'-'C' - 2 PLACES -

SECTION 'D'-'D' - 2 PLACES -

4. ENERGY DISCHARGE

An investigation of energy discharges was initiated using the torodial coil discussed in the first part of this report. The experiments on this coil have not yet been completed, but the results obtained to date will be discussed.

The test circuit is shown in Fig. 12. With S closed, R is adjusted so that the desired coil current is obtained. A certain quantity of energy is then stored in L. Since a suitable discharge switch is not yet available, the persistent current mode of operation was eliminated and discharge initiated by opening S. The output pulse characteristics can be controlled by means of the discharge capacitor C and load resistor R_L. The transient solution of the circuit equation

$$C \frac{dE}{dt} + \frac{E}{R} + \int \frac{E}{L} \, dt = 0 \qquad (15)$$

yields after solving for E,

$$E = \frac{I_o}{C} t \, e^{-\alpha t} \qquad (16)$$

For critical damping:

$$\alpha = \frac{1}{2RC} \quad \text{and} \quad \frac{4R^2 L}{C} = 1$$

Differentiation of (16) to t and equating to 0 gives:

$$t_m = 2RC \qquad (17)$$

$$E_m = \frac{2}{e} I_o R \qquad (18)$$

in which t_m is the time in which the maximum voltage E_m is obtained. This is presented by curve a in Fig. 13. Curves b and c of Fig. 13 represent under-damped and over-damped oscillations respectively.
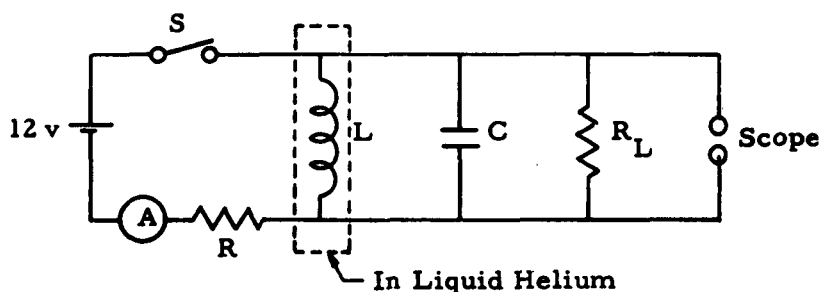
Fig. 12   Test Circuit for Energy Discharge Experiments
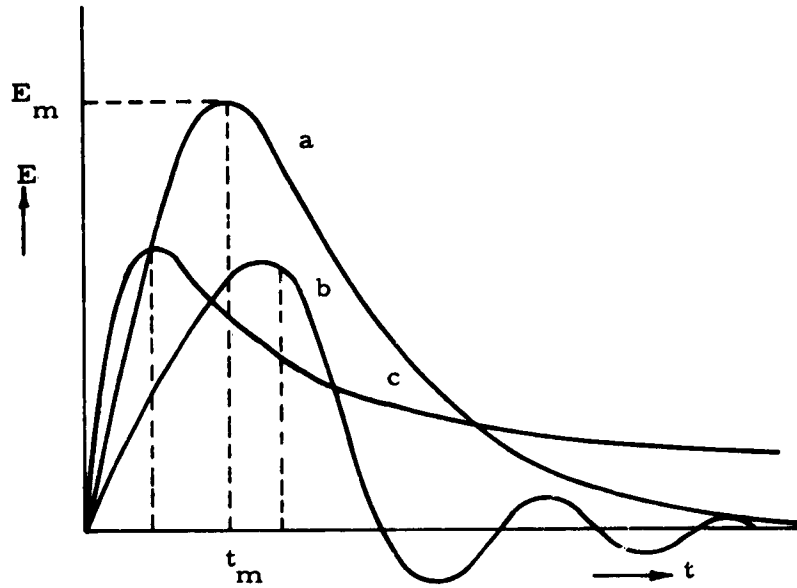
**Fig. 13 Discharge Voltages for the Critically Damped (a),
Under-Damped (b) and Over-Damped (c) cases.**

For the under-damped case:

$$E = \frac{2 I_o R}{\sqrt{\frac{4R^2 C}{L} - 1}} \, e^{-\frac{t}{2RC}} \quad \sin \, \frac{t}{2RC} \sqrt{\frac{4R^2 C}{L} - 1} \tag{19}$$

$$E_{max} = \sqrt{\frac{L}{C}} \; I_o \; \exp \left\{ \left(\frac{-1}{\sqrt{\frac{4R^2 C}{L} - 1}} \right) \left(\tan^{-1} \sqrt{\frac{4R^2 C}{L} - 1} \right) \right\} \tag{20}$$

$$t_{max} = \frac{2RC}{\sqrt{\frac{4R^2 C}{L} - 1}} \; \tan^{-1} \left(\sqrt{\frac{4R^2 C}{L} - 1} \right) \tag{21}$$

4.1   TEST RESULTS

An oscillograph of a discharge using the circuit of Fig. 12 where
$L \simeq 0.14$ h, $R_L = 100 \, \Omega$, $I_o = 3$ amps and $C = 50 \mu f$ is shown in Fig. 14. A
similar oscillograph for $C = 20 \mu f$ is shown in Fig. 15.

21
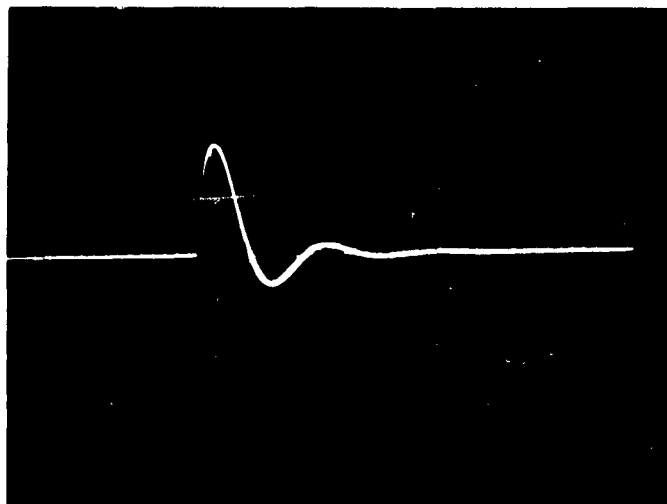
E 50v/scale div.

t 10 msec/scale div.

Fig. 14 Output Pulse for $L \simeq 0.14H$, $R_L = 100\,\Omega$, $I_o = 3$ amps and $C = 50\,\mu f$

E 50v/scale div.
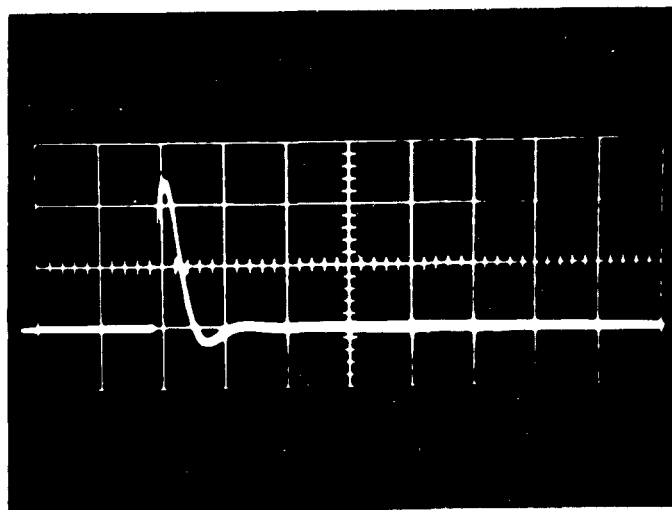
t 10 msec/scale div.

Fig. 15 Output Pulse for $L \simeq 0.14H$, $R_L = 100\,\Omega$, $I_o = 3$ amps and $C = 20\,\mu f$

22

Calculation of $\dfrac{4R^2 C}{L}$ for the values of C indicates that both waveforms are underdamped or oscillatory. This is also clearly indicated by Figs. 14 and 15. Thus both discharges are represented by Eq. (19). The total energy discharge can be calculated from:

$$Q = \int_0^\infty \frac{E(t)^2}{R_L} \, dt \tag{22}$$

where   Q = energy dissipated (joules)
         R_L = load resistance (Ω)

E(t) can be represented by:

$$E(t) = a \, e^{-bt} \sin c t \tag{23}$$

where a, b and c are constants defined by Eq. (19). Substituting (23) in (22) and integrating over t yields the total energy dissipated.

If a, b and c are calculated from the circuit parameters and Eq. (19), the calculated Q would represent the total stored energy. In order to find the dissipated energy, a, b and c must be related to E_m and t_m as obtained from the oscillographs.

At $t = t_1 = $ time to complete first half cycle,

$$\sin c \, t_1 = 0$$

At $E = E_m$, $\dfrac{dE}{dt} = 0$ and $t = t_m$.

Equation (23) can then be represented by:

$$E = E_m \, e^{\alpha(t_m - t)} \sin \beta t$$

$$\alpha = \beta \, \frac{\cos \beta \, t_m}{\sin \beta t_m} \tag{24}$$

$$\beta = \frac{\pi}{t_1}$$

Substituting in (22) yields

$$Q = \frac{(\beta E_m)^2}{4 R_L \alpha} \left(\frac{1}{\alpha^2 + \beta^2} \right) \tag{25}$$

From Fig. 14 we find:

$$E_m \simeq 95 \text{ V}$$
$$t_m \simeq 4 \times 10^{-3} \text{sec.}$$
$$t_1 \simeq 10^{-2} \text{ sec.}$$

Substituting in Eq. (25) yields:

$$Q = 0.46 \text{ joule.}$$

The stored energy was:

$$Q_{stored} = 1/2 \ (0.14) \ (3)^2 = 0.63 \text{ joule}$$

indicating an efficiency of 73%.

These results are by no means conclusive or accurate. In the first place the inductance L was not accurately known. L was measured with a General Radio bridge but since L= f(B) the measurement should be made at a DC current of 3 amps. Furthermore, E_m and t_m were taken from the oscillograph and are subject to some error in interpretation. However, a high efficiency was expected since the coil did not go normal during switching. The discharge was made from an initial coil current of 3 amps, which is well below the critical current. The tests will therefore be repeated at currents just below I_c for this coil. The reason why this was not done is that arcing problems were encountered in the switch. A fast acting high voltage switch is presently being developed for these tests.

4.2   FUTURE PROGRAM

The energy discharge experiments on the toroid will be continued. The availability of a better discharge switch will allow discharges involving larger quantities of energy and at higher voltages and shorter discharge times. As soon as the solenoid for short wire tests is completed, this coil will also be used for discharge experiments. The solenoid is expected to store up to 400 joules, allowing high voltage discharges to be made.

5. VACUUM INSULATION STUDIES

5.1   VACUUM BREAKDOWN STUDIES

During the period covered by this report, experiments have been made with a high voltage bushing terminated by a field intensification disc (see Fig. 14, Fourth Quarterly Technical Note).   The purpose of these experiments was to observe the effect on the bushing's voltage holding capability of the field intensification at the edge of the disc, and to determine if a "critical" radius existed for this edge, below which value the voltage on the bushing was severely limited by field emission. The maximum voltage supported by the bushing was measured for three positions of the disc relative to the center of the chamber, for both bushing polarities, and at two ambient pressures (10^{-4} and 10^{-7} torr). Table IV shows the experimental results.

It is apparent that voltages at 10^{-4} torr are much higher than at 10^{-7} torr, a fact which has been observed and remarked upon previously. The reasons for this pressure effect are still not known, but from consideration of electrode gaps and the ambient pressure, this does not seem to be directly a mean free path phenomenon. It is also clear that alteration of the radius had little effect on the bushing voltage when the bushing was positive, but that when the bushing was negative, this voltage did decrease with decreasing radius of the edge of the disc. This can be understood in terms of the Fowler-Nordheim field emission theory (see Fifth Quarterly Technical Note), because field emitting electrons (from a negative surface) occurs at lower microscopic field strengths than are necessary for field emission of positive ions.   As the radius of the edge of the disc is decreased, the electric field existing at that edge for a given bushing voltage is increased, and electron emission due to this field may occur if the bushing is negative with respect to the vacuum chamber.

When the disc was some 20 cm away from the center of the vacuum chamber the edge was to some extent protected by the end of the bushing itself, so that the field at the edge was somewhat less than when the disc was at the center of the chamber. This accounts for the decrease in voltage as the discs were moved from the 23 cm to the zero cm positions.

These results do not reveal the existence of a critical radius for the edge of the disc, and it is planned to test two more discs in a similar manner. These discs will have edges of 0.05 and 0.02 cm respectively.

TABLE IV

Voltage supported (kv) by a high voltage bushing when terminated with a field intensification disc having an edge of known radius.

Distance of disc from center of vac. chamber cm	Radius of curvature of the disc edge, cm			
	0.64	0.32	0.23	0.11

At $p \sim 10^{-4}$ torr, disc having positive polarity

23	1120 kv	1200 kv	870 kv	1030 kv
10	1050	1110	1000	1010
0	1030	1100	1020	1030

At $p \sim 10^{-4}$ torr, disc having negative polarity

23	920	830	880	610
10	880	740	690	470
0	830	710	720	600

At $p \sim 10^{-7}$ torr, disc having positive polarity

23	400	400	480	410
10	290	310	340	280
0	280	300	330	280

At $p \sim 10^{-7}$ torr, disc having negative polarity

23	630	540	570	480
10	610	590	600	460
0	590	570	450	400

More measurements have been made of the breakdown voltage V as a function of electrode separation d, for 304 stainless steel electrodes having essentially sphere-to-plane geometry. The diameters of the spheres were $1/16''$ and $2''$ respectively, and measurements were made at ambient pressures of 10^{-4} and 10^{-7} torr. Because of leaks in the forepumping line, all of the data for the $2''$ sphere at 10^{-4} torr could not be taken. However, this will be completed during the coming period, together with similar tests on a $3/8''$ diameter sphere. 35 mm slides, numbers 173 and 174 (already sent to Eglin AFB), show these and other spherical electrodes.

Table V shows the experimental results for the $1/16''$ and $2''$ sphere. Again it can be seen that voltages are higher at p $\sim 10^{-4}$ torr than at p $\sim 10^{-7}$ torr, and for the $1/16''$ sphere when it is positive rather than negative. For the $2''$ sphere, V is slightly higher when the sphere is negative rather than positive. However, there is little field intensification at the surface of the $2''$ sphere, since its radius is relatively large, so that the slight differences in voltage for the two polarities are not regarded as field emission effects. The $1/16''$ sphere does show these effects because of the strong intensification at its surface. Thus the voltage is lower when the sphere is a cathode and emits electrons. It was interesting to observe that when this small sphere was an anode and the electrode separation < 2 cm, it glowed red under the bombardment of copious electrons from the large cathode.

V as a function of d has been measured for pairs of $8''$ diemater, $20''$ radius of curvature electrodes, the anode of which was 304 stainless steel buffed to a good polish while the cathode was of 304 stainless steel or aluminum coated with an organic or an inorganic material. Slide number 175 shows some of these coated electrodes, while experimental results are tabulated in Table VIa and VIb.

Of the first three coatings investigated, only Durafilm Enamel #300 gave other than poor results, and it is felt that this enamel should be tried again at a later date. The other two coatings were 4 mils of clear Teflon applied over a green primer, and about 5 mils of Kel F coating, which is a material similar to Teflon. Both of these coatings gave substantially lower values for V than were obtained with the enamel coating. The nature of the enamel is not known, but it probably bears some similarity to the silicon oxide coating already examined (see Fig. 25, Fifth Quarterly Technical Note).

Table VII shows V = f(d) for a pair of 304 stainless steel electrodes, $8''$ diameter and $20''$ radius of curvature, buffed to a good polish, at $\sim 10^{-7}$ torr ambient pressure. These tests were made with a variety of bushing configurations which are discussed below. Average values for V are also shown in Table VII, and apart from the values at 1 cm and 20 cm, these appear to follow the

TABLE V

Vacuum breakdown voltage V as a function of electrode separation d for 304 stainless steel electrodes having essentially sphere-to-plane geometry. The spherical electrodes were 1/16" and 2" in diameter, while the opposing electrode was 8" in diameter, 20" radius of curvature.

Ambient pressure torr	Electrode separation cm	Breakdown voltage, kv	
		Sphere positive polarity	Sphere negative polarity
	1/16" diameter sphere		
10^{-4}	20	1440	920
	10	1160	500
	6	1160	370
	4	1110	440
	2.5	1030	370
	1.5	760	340
	1.0	600	325
10^{-7}	20	720	620
	10	690	380
	6	700	230
	4	660	210
	2.5	620	170
	1.5	610	150
	1.0	500	150
	0.5	430	-
	2" diameter sphere		
10^{-4}	20	-	1270
	10	-	1160
	6	-	920
10^{-7}	20	590	690
	10	600	680
	6	530	670
	4	510	650
	2.5	440	570
	1.5	400	490
	1.0	420	450

TABLE VI a

Vacuum breakdown voltage V as a function of electrode separation d for 8"
diameter, 20" radius of curvature electrodes, the anode of which was 304
stainless steel while the cathode was aluminum coated with Teflon, Kel F
or Durafilm Enamel #300.

Ambient pressure, torr	Electrode separation, cm	Breakdown voltage, kv		
		Teflon coating	Kel F coating	Enamel #300 coating
10^{-6}	20*	360	340	490
	10	390	180	510
	6	220	80	520
	4	110	30	480
	2.5	80	-	260
	1.5	-	-	150
	1.0	60	-	80

*Measurements were made in the order shown. All of the coatings showed a
 puncture mark on subsequent examination, and this raises the question
 whether the low voltages obtained for Teflon and Kel F at small gaps were
 caused by prior damage to the coating.

TABLE VI b

Vacuum breakdown voltage V as a function of electrode separation d for 8" diameter, 20" radius of curvature electrodes, the anode of which was 304 stainless steel while the cathode was aluminum or 304 stainless steel, coated with MgF_2.

Ambient pressure $\sim 10^{-7}$ torr

Electrode separation, cm	Breakdown voltage, kv			
	MgF_2 on S.S.	MgF_2 on S.S.	MgF_2 on Al	MgF_2 on Al
40	-	510	-	-
20	480	430	470	-
10	320	360	430	670
6	310	320	400	390
5	-	-	-	350
4	300	300	310	330
2.5	280	280	310	310
2.0	-	270	-	-
1.5	220	250	280	-
1.0	210	240	250	-

TABLE VII

Vacuum breakdown voltage V as a function of electrode separation d for a pair of 8" diameter, 20" radius of curvature 304 stainless steel electrodes, at $p \sim 10^{-7}$ torr.

Electrode Separation, cm	Breakdown Voltage V kv								Average Values
	Test #'s								
	A	B	C	D	E	F	G	H	
20	610	-	-	-	-	510	450	520	520
18	-	620	665	710	-	-	-	-	665
10	550	520	510	550	-	620	360	470	510
6	530	480	370	500	480	560	330	430	460
4	490	460	250	420	420	530	330	-	415
2.5	460	390	170	400	380	400	330	380	360
1.5	410	280	100	320	335	270	310	350	300
1.0	340	180	65	-	-	170	200	210	195

Bushing Configurations:

Test #	Bushing #2	Bushing #3
A	1/8" field rings, aluminum dome, Adiprene urethane resistor	as Bushing #2, Test A.
B	1/8" field rings, aluminum dome, Conap urethane resistor	3/4" field rings, interlocking shields over electrode shaft, Adiprene urethane resistor
C	1/8" field rings, two shielding cones with apexes toward electrode, Conap urethane resistor	as Bushing #3 in Test B
D, E	as Bushing #2 in Test C, but with apexes of cones toward generator	1/8" field rings, interlocking shields over electrode shaft, Adiprene urethane resistor
F	as Bushing #2, Test D	as Bushing #2, Test A
G, H	as Bushing #2, Test D, but with electrodes surrounded by open-ended glass box	as Bushing #2, Test A, but with electrodes surrounded by open-ended glass box

relation $V = kd^{\alpha}$, where $\alpha \approx 0.31$ and $k \approx 2.6$ kv/cm[31]. Thus, the gradient of the straight line obtained when log V is plotted against log d is somewhat less than that of the Trump-Van de Graaff line[8], although the latter refers to small electrodes.

The individual voltages supported by each bushing during the tests A - H indicate that the interlocking shields used to cover the electrode shaft of bushing #3 do not improve the performance of that bushing, from which it can be concluded that the performance of the bushings is not at present affected by field intensifications at the electrode shaft. It has already been remarked upon (Fifth Quarterly Technical Note) that the 3/4" field rings give slightly higher voltages than the 1/8" rings, but that the conditioning time for the former is longer than for the latter. A bushing with 3/4" field rings is shown in Fig. 27 of the Fifth Quarterly Technical Note.

Figure 29 of the same report shows a bushing with the same configuration as bushing #2 in test C. The purpose of these truncated cones was to shield the glass insulator rings of the bushing from particle bombardment. That this was effective to some extent was shown by the improved voltage stability of the bushing. Reversing the cones so that their apexes now pointed toward the generator (see 35 mm slides #170 and 171) resulted in the same improved stability, but with higher total voltages (see Table VIII). With the latter configuration, the surfaces of the cones follow closely the equipotential surfaces that exist inside the vacuum chamber when the cones are removed.

Tests G and H were made with an open-ended glass box inside the vacuum chamber, so that the electrodes projected into the box and were thus shielded by the glass from direct particle bombardment from the vacuum chamber wall. It had been suggested[9] that such bombardment might account for the low total voltages that could be supported between the electrodes, and that the presence of the glass box might substantially raise these voltages. Comparison between test F and tests G and H show that this is not the case. The presence of the glass box tends, in fact, to give lower total voltages than are obtained without it.

The Conap and Adiprene urethane used for the bushing resistors had a specific resistivity of 1×10^{11} and 1×10^{12} Ω cm respectively. The Conap resistor therefore carried more current than the Adiprene resistor at a given voltage and, hence, the voltage grading of the bushing surfaces was improved. This seemed to give stability to the bushing. Table IX shows the total charging current to the belt of the Van de Graaff generator as a function of the total voltage supported by a bushing with a Conap urethane resistor. The maximum voltage on the bushing was 450 kv, at which point further increase in charging current did not affect the voltage (current loading phenomena). The corresponding charging current was about 120 μa.

TABLE VIII

Highest total voltages supported at $\sim 10^{-7}$ torr by a bushing with some insulating rings shielded by two truncated cones.

Bushing Polarity	Voltages Supported, kv	
	(a) with apexes of cones toward electrode	(b) with apexes of cones toward generator
+	300	330
-	540	600

TABLE IX

Tabulation of the total charging current to the belt of a Van de Graaff generator and the corresponding voltage supported by a bushing at an ambient pressure of 10^{-7} torr.

Belt charging current μa	Bushing voltage, kv
25	100
50	200
75	290
100	380
125	450
150	450

In this experiment, the high voltage bushing had a resistor of Conap urethane. Onset of current loading phenomena occurred at about 120 μa charging current. Below this point, voltage rose linearly with charging current, and above this point it was essentially independent of charging current.

5.2 TYPE II BUSHING

The parts for a complete Type II Bushing have been fabricated. 35mm slides #176, 177 and 178 show the completed glass and stainless steel insulator stack which will support high voltage in vacuum. The corresponding support of high voltage in the pressurized medium of the generator will be done with a modified cylinder of cast urethane-epoxy. A sample of this urethane-epoxy has been pressure-tested to 1800 psi without failure, while the piece itself has been pressure-tested to 300 psi satisfactorily. The internal bushing pressure will be about 150 psi, but in normal operation, the pressure differential across the wall of the urethane cylinder should only be $\sim$ 10 psi.

The bushing has been assembled and pressure-tested to 250 psi. It is hoped to voltage-test it in the near future.

5.3 HIVE FACILITY

The high vacuum, high electric field facility - HIVE - has been fabricated. This facility has two modified feedthrough bushings which are expected to hold up to 200 kv each in vacuum, giving the facility a capability of 400 kv. At present, the vacuum system associated with the facility is being assembled.

It is expected that a study of electrode materials, electrode coatings and surface finishes will be carried out in the facility, which is instrumented to measure the pre-breakdown currents between electrodes.

5.4 FACILITY MAINTENANCE

Every aspect of the facility has been inspected or overhauled and is being reassembled. This maintenance has appeared necessary for some time, and the recent delivery of the 12" pumping system has created a suitable opportunity. It has included buffing of the inside of the vacuum chamber, fabrication of a new control panel and forepumping line, and thorough cleaning of both Van de Graaff generators. A leak-valve has also been installed, so that pressure in the vacuum chamber can be varied from 1×10^{-7} to 1×10^{-1} torr and kept constant.

5.5 FUTURE PROGRAM

The immediate program is concerned primarily with installation of the new pumping system and finishing work on the maintenance of the facility. When this is done, high voltage tests will be continued. In particular, the effect

35

of installing a shield on the bushing will be tried so that the high potential end of the bushing views this shield (which will be at half the bushing potential) rather than the walls of the vacuum chamber. This shield is shown in 35mm slides #168 and 169.

It is hoped to examine the effect of using a urethane resistor to give non-linear voltage grading of the bushing surface in vacuum. A special two-material resistor has been cast for this purpose.

6. REFERENCES

1. Montgomery, D. B., "Current Carrying Capacity of Superconducting Nb-Zr Solenoids," National Magnet Laboratory, M. I. T., Cambridge, Mass., Contract AF19(604)-7344.

2. LeBlanc, M. A. R., and Little, W. A., "Proceedings of the International Conference of Low Temperature Physics," University of Toronto Press, p. 362, 1961.

3. Hulm, J. K., Chandrasekhar, B. S., and Riemersma, H., Conference Paper, Cryogenics Conference, Los Angeles, Calif., August 1962.

4. Fifth Quarterly Technical Note, "Power Sources for Directed Energy Weapons," AF08(635)-2166 (S).

5. Meissner, W., and Ochsenfeld, R., "Naturwiss," 21, 787, 1933.

6. Meissner, H., Phys. Rev. 109, No. 3, 686, 1958.

7. Meissner, H., Phys. Rev. 117, No. 3, 672, 1960.

8. Trump, J. G., and Van de Graaff, R. J., J. App. Phys. 18, 327, 1947.

9. Trump, J. G., M. I. T. (private communication).

INITIAL DISTRIBUTION

1	Wpns Sys Eval Gp	1	5AF (5FOPR-RQ)
1	Hq USAF (AFRDR-NU-3)	1	AFCRL (CRRDA)
1	Hq USAF (AFORQ-OT)	1	AFLC (MCD)
1	Dep IG for Insp (AFIPA)	1	RADC (RCLMS)
1	Def Dir of R&E	1	RADC (Tech Lib)
5	Dir Advanced Rsch Proj Agency	2	AEDC (Tech Lib)
1	DASA (Doc Lib Br)	1	AFSP Comm Cen (SCP)
1	DOFL	1	AFFTC (FT-OOT)
1	AFSC (SCGN)	1	PACAF (PFORQ)
1	AFSC (SCSA)	2	AFSWC (Tech Lib)
1	AFSC (SCFTA)	1	AFMTC (MTASI)
1	AFSC (SCTAE)	1	Elec Sys Div (ESRD)
3	ASD (ASAPRL-Lib)	1	MAAMA (MANE)
1	ASD (ASAT-Index)	1	OOAMA (OOY)
2	ASD (ASRNG)	1	USAFSS (CLR)
1	ASD (LMSE)	1	USAFSS (DCS/OPS)
1	ASD (ASRSMD)	1	Ballistic Resch Lab (Lib)
2	ASD (ASRNGW)	1	Frankford ARS (Lib)
3	ASD (ASAPT)	1	Lake City ARS (IED-ORDOM)
3	SSD (SSPRE)	1	US Atomic Energy Comm
2	SSD (Tech Lib)		(Tech Info Ex)
2	BSD (Tech Lib)	1	1 Strat Aerospace Div
2	BSD (BSTE)	1	AF Tech Applications Cen/TD
2	BSD (BSQ)	1	OPNAV (OP-75)
1	ESD (Tech Lib)	2	OPNAV (OP-76)
1	AAC (ACS/Intell)	2	BUWEPS (RT)
1	AWS (TIPD)	1	Off of Naval Resch (Physics Div)
1	AAC (OA)	1	BUSHIPS (Code 335)
1	AAC (XPR)	1	US Naval Ord Lab (Lib)
1	ADC (MME)	1	US Naval Wpns Lab (Lib)
1	SAC (DIT)	1	US Naval Ord Lab)
1	SAC (DM4A)	2	US Naval Resch Lab (Code 6240)
1	SAC (DPLBC)	1	US Naval Ord Test Sta (Lib)
1	SAC (DOCEO-T)	1	NAMTC
1	SAC (DOPLT)	1	Marine Corps Eq Bd
1	SAC (DOROM)	1	US Army Cml Corps Fld
1	SAC (DOSD)	1	Chief of Ordnance (ORDTS)
1	SAC (OA)	1	OAR (Lib)
2	TAC (DORO)	1	OAR (RRY)
2	TAC (DO)	1	US Cml Corps Proving Grnd
1	ATC (ATTWS)	1	US Army Cml Corps Nuclear
1	Atomic Wpn Tng Cmd (DASA)		Def Lab
1	5AF (5FAG-P)	1	US Army Cml Corps R&D Lab
2	FTD (FT4C)		(Lib)

INITIAL DISTRIBUTION (Continued)

1	US Army Cml Corps Biological Lab
1	Off of Ord Resch US Army (ORDOR-IR)
1	Tech Info Sec (Ord Corps)
1	Picatinny Arsenal (RDBB-VC2)
1	ABMA (ORDAB-HT)
1	ARGMA (Tech Lib)
1	Ballistic Resch Lab
1	Gen Elec Tempo Div
1	Raytheon Co
5	Ion Physics Corp
1	Aerojet-Gen Corp
1	Dir USAF Proj RAND
1	AU (AUL-9764)
15	ASTIA (TIPCR)
	APGC
6	PGAPI
1	PGF
1	TACLO
15	ASQWR

Det 4, Aeronautical Systems Division, Eglin Air Force Base, Florida
Rpt No. ASD-TDR-63-14, POWER SOURCES FOR DIRECTED ENERGY
WEAPONS, Sixth Qtrly rpt, April 1963, 39p. incl illus., tables, 9 refs.
Unclassified report

A discussion is given of initial test results obtained on a superconducting toroidal coil and a thermal discharge switch. Critical currents of the toroid are very high at low fields but considerable current degradation was observed at fields in the order of 15 kilogauss. Initial test results on the thermal switch indicate that the time required for a thermal transition is rather long (1/2 sec). More tests are to be performed, including an investigation of magnetic transitions. Some discharge experiments have been performed. Low energy discharge pulses with a rise time in the order of 2 msec have been obtained. Experiments are described in which the vacuum breakdown voltage as a function of electrode separation were measured for simultaneous 304 stainless steel electrodes having essentially planar geometry, for similar electrodes having the cathode coated with a variety of materials, and for electrodes having sphere-to-plane geometry. Electrode separation was varied between 20 and 1 cm, while the ambient gas pressure was either about 10^{-4} or 10^{-7} torr. In other experiments at these pressures, the voltage support capability of the high voltage bushing has been measured when it is terminated by field intensification discs (having an edge of known radius of curvature), and when some of the bushing's glass insulator rings are protected by two truncated cones. A urethane grading resistor having a specific resistivity 1×10^{11} ohm-cm was used in one of the bushings during some of these tests. The 400 kv HIVE facility, in which complementary vacuum breakdown studies will be carried out, has been assembled and the high voltage bushings satisfactorily tested. Latest progress in the development of the Type II high voltage bushing is described. It is hoped to voltage-test the first of these bushings shortly.

1. Plasma physics
2. Space weapons
I. AFSC Project 3805
II. Contract AF 08(635)-2166
III. Ion Physics Corp.,
      Burlington, Mass.
IV. Secondary Rpt No. 6th Qrty Rpt
V. In ASTIA collection

Det 4, Aeronautical Systems Division, Eglin Air Force Base, Florida
Rpt No. ASD-TDR-63-14, POWER SOURCES FOR DIRECTED ENERGY
WEAPONS, Sixth Qtrly rpt, April 1963, 39p. incl illus., tables, 9 refs.
Unclassified report

A discussion is given of initial test results obtained on a superconducting toroidal coil and a thermal discharge switch. Critical currents of the toroid are very high at low fields but considerable current degradation was observed at fields in the order of 15 kilogauss. Initial test results on the thermal switch indicate that the time required for a thermal transition is rather long (1/2 sec). More tests are to be performed, including an investigation of magnetic transitions. Some discharge experiments have been performed. Low energy discharge pulses with a rise time in the order of 2 msec have been obtained. Experiments are described in which the vacuum breakdown voltage as a function of electrode separation were measured for simultaneous 304 stainless steel electrodes having essentially planar geometry, for similar electrodes having the cathode coated with a variety of materials, and for electrodes having sphere-to-plane geometry. Electrode separation was varied between 20 and 1 cm, while the ambient gas pressure was either about 10^{-4} or 10^{-7} torr. In other experiments at these pressures, the voltage support capability of the high voltage bushing has been measured when it is terminated by field intensification discs (having an edge of known radius of curvature), and when some of the bushing's glass insulator rings are protected by two truncated cones. A urethane grading resistor having a specific resistivity 1×10^{11} ohm-cm was used in one of the bushings during some of these tests. The 400 kv HIVE facility, in which complementary vacuum breakdown studies will be carried out, has been assembled and the high voltage bushings satisfactorily tested. Latest progress in the development of the Type II high voltage bushing is described. It is hoped to voltage-test the first of these bushings shortly.

1. Plasma physics
2. Space weapons
I. AFSC Project 3805
II. Contract AF 08(635)-2166
III. Ion Physics Corp.,
      Burlington, Mass.
IV. Secondary Rpt No. 6th Qrty Rpt
V. In ASTIA collection